Acta Pharmaceutica Sinica B 2017;7(3):326–333

Chinese Pharmaceutical Association
Institute of Materia Medica, Chinese Academy of Medical Sciences

Acta Pharmaceutica Sinica B

www.elsevier.com/locate/apsb
www.sciencedirect.com

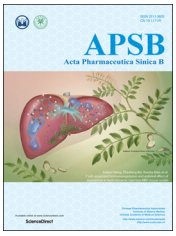

ORIGINAL ARTICLE

Establishment of a new acute-on-chronic liver failure model

Fangfang Li[a], Luyang Miao[b], Hua Sun[a,*], Yuyang Zhang[b], Xiuqi Bao[a], Dan Zhang[a,*]

[a]*State Key Laboratory of Bioactive Substance and Function of Natural Medicines, Institute of Materia Medica, Chinese Academy of Medical Sciences & Peking Union Medical College, Beijing 100050, China*
[b]*Shenyang Pharmaceutical University, Shenyang 110016, China*

Received 10 July 2016; received in revised form 31 August 2016; accepted 18 September 2016

KEYWORDS

ACLF;
D-Galactosamine;
Fibrosis;
Lipopolysaccharide;
Porcine serum;
Rat

Abstract To establish an animal model of acute-on-chronic liver failure (ACLF) that would replicate the pathological process of ACLF in humans, rats were administered porcine serum (PS) for 11 weeks. Liver fibrosis was determined by pathological and biochemical assessments. The animals then were injected with D-galactosamine (D-gal) and lipopolysaccharide (LPS). The survival times of animals with cirrhosis and ACLF were determined over 48 h. Other animals were killed at 0, 4, 8 and 12 h after administration of D-gal/LPS. Liver injury was assessed by histopathological analysis and biochemical indices, and apoptosis was detected by Western blot and TUNEL analysis. After PS administration for 11 weeks the serum levels of hyaluronic acid and N-procollagen type III peptide increased significantly, and serious fibrosis and cirrhosis was observed at weeks 10 and 11. Cirrhotic rats were injected with D-gal/LPS to induced ACLF; the rate of mortality over 48 h was 80%. ALT and AST levels increased markedly at 4 h, but decreased significantly at 8 and 12 h post-treatment. The total bilirubin, direct bilirubin, and total bile acids levels increased markedly at 8 and 12 h. Clotting times, TNF-α and IL-6 levels increased significantly, except for 12 h post-treatment. Apoptosis, inflammation and necrosis were elevated as determined by hematoxylin-eosin staining and TUNEL assays. BCL-2 levels decreased significantly, While BAX levels increased significantly. Cytochrome *c* expression peaked at 8 h post-D-gal/LPS treatment. In conclusion, an ACLF model induced by PS and D-gal/LPS was established and the underlying mechanisms of ACLF development were explored.

*Corresponding authors. Tel.: +86 10 63165203; fax:+861063017757.
E-mail addresses: sunhua@imm.ac.cn (Hua Sun), danzhang@imm.ac.cn (Dan Zhang).

Peer review under responsibility of Institute of Materia Medica, Chinese Academy of Medical Sciences and Chinese Pharmaceutical Association.

http://dx.doi.org/10.1016/j.apsb.2016.09.003

1. Introduction

Acute-on-chronic liver failure (ACLF) has generated increasing attention in recent years. In 2009, the Asian Pacific Association for the Study of the Liver defined ACLF as an acute hepatic insult manifesting as jaundice and coagulopathy, becoming complicated within 4 weeks by ascites and/or encephalopathy in a patient who was previously diagnosed or undiagnosed chronic liver disease[1]. The characteristic features of ACLF include a rapid progression, the requirement for multiple organ supports, and a high incidence of short- and medium-term mortality (50%–90%)[2]. In a large-scale study[3] conducted from 2000 to 2004 in China, 77.3% (618/799) of patients with liver failure were diagnosed with ACLF and cirrhosis. Among the patients with ACLF, 96.76% (598/618) had HBV infection.

Effective treatments for ACLF are lacking[4]. The pathophysiological background of ACLF remains poorly understood, necessitating the development of optimal experimental ACLF models with features resembling those of the human disorder. The most widely used ACLF model is induced in rats[5] and mice (Pko and Pwt mice)[6] by human serum albumin (HSA) and D-galactosamine (D-gal)/lipopolysaccharide (LPS), which serve as reliable mimics for the pathophysiological processes and histological characteristics of ACLF, while the HSA-induced model shows relatively high mortality with fibrosis. Balasubramaniyan et al.[7] developed an ACLF model using a bile-duct ligation (BDL) method. Hou et al.[8] used CCL_4 and D-gal/LPS to establish an ACLF model. However, these two models are not entirely consistent with the pathogenesis of ACLF, and the operation required for the BDL model is difficult.

In this study we developed a new rat model of ACLF based on the method of Yang et al.[9]. To reduce the death rate in rats following HSA administration, we used PS to induce chronic immune liver cirrhosis, for which the pathogenesis was consistent with HBV infection. Subsequent injection of D-gal and LPS established the ACLF model. We utilized this model to explore the characteristics and mechanisms underlying ACLF.

2. Materials and methods

2.1. Experimental animals

Wistar rats weighing 120–150 g were obtained from Beijing Weitonglihua Experimental Animal Co., Ltd. (Beijing, China). They were housed in an environmentally controlled room (20 ± 3 °C, 50 ± 20% humidity, 12-h light/dark cycle) with free access to food and water. Animal care and all experimental procedures were approved by the Animal Ethics Committee at Chinese Academy of Medical Sciences & Peking Union Medical College, and conducted in accordance with the health criteria for care of laboratory animals enacted by the Beijing municipal government.

2.2. Establishment of ACLF models

Male Wistar rats were randomly divided into 2 groups (control: $n=10$; ACLF model: $n=60$). Rats in the ACLF group were administered porcine serum (Beijing Solarbio Science &Technology Co., Ltd., Beijing, China) intraperitoneally at a dose of 0.5 mL twice per week for 11 weeks to generate an immune liver fibrosis model. After 11 weeks, rats with immune liver fibrosis were injected intravenously with LPS (Sigma-Aldrich Co., USA) at a dose of 50 μg/kg. Thirty minutes later, D-gal (Sigma-Aldrich Co., USA) was injected intraperitoneally at a dose of 600 mg/kg to induce acute liver failure *via* chronic liver cirrhosis. The control group was administered physiological saline at the same time points. Animals were killed at 0, 4, 8 and 12 h post-treatment for blood and hepatic tissue collection. The remaining rats were observed for survival time every hour for 48 h.

2.3. Measurement of fibrotic markers

Hepatic hydroxyproline (Hyp) levels were determined using a hydroxyproline assay kit obtained from Nanjing Jiancheng Corp. (Nanjing, China), according to manufacturer's instructions. Serum levels of hyaluronic acid (HA) and N-procollagen type III peptide (PIIINP) were assayed using an ELISA kit obtained from Beijing Fangcheng Biotech, according to manufacturer's instructions.

2.4. Ultrasound analysis

At 6, 8, and 10 weeks following porcine serum injection, five rats were randomly selected and ultrasonography (US) was performed to estimate the degree of fibrosis. Before the day of examination, animals were fasted overnight but were given free access to water. Animals were anesthetized using pentobarbital sodium (50 mg/kg) and their abdomens were shaved to reduce imaging artifacts. A sound-conducting gel (Carbogel®, Brazil) was applied and an US examination was performed using a micro-ultrasound system (VisualSonics, Canada). The animals were examined in the supine position to assess the liver. The same transverse cross sections were held constant throughout the experiments.

2.5. Determination of serum biochemical indices

Blood samples were collected in tubes and centrifuged for 15 min at 3500 rpm (Sigma, USA) to collect serum. The serum levels of alanine aminotransferase (ALT), aspartate aminotransferase (AST), total bilirubin (TBiL), direct bilirubin (DBiL), and total bile acids (TBA) were detected with an automatic analyzer (Toshiba, Japan) using commercial kits (the ALT/GPT Kit, AST/GOT Kit, TBiL Kit, and DBiL Kit) from Zhongsheng Beikong Co., Ltd. (Beijing, China) according to manufacturer's instructions.

2.6. Determination of prothrombin times (PTs)

Blood samples were collected in anticoagulant tubes containing sodium citrate solution and centrifuged for 15 min at 3500 rpm (Sigma, USA) to collect plasma. Clotting time was measured using a kit obtained from Nanjing Jiancheng Corp. (Nanjing, China) according to manufacturer's instructions.

2.7. Determination of plasma ammonia levels

Blood samples were collected in anticoagulant tubes containing heparin sodium and plasma ammonia measurements were performed with a kit obtained from Nanjing Jiancheng Corp. (Nanjing, China) by following the manufacturer's instructions.

2.8. Measurement of TNF-α and IL-6 production by ELISA

Blood samples were collected in tubes and centrifuged for 15 min at 3500 rpm to collect serum. The serum levels of TNF-α and IL-6 were determined using a commercial enzyme-linked immunosorbent assay (ELISA) kit (Neobioscience Technology, Shenzhen, China) following the manufacturer's instructions.

2.9. Histological examinations

Liver tissues were fixed in paraformaldehyde solution. The tissue samples were processed using paraffin block techniques in wax, deparaffinization in xylene, and dehydration in alcohol. The samples were then sectioned (>5 μm) and stained with hematoxylin-eosin (H&E) to evaluate the pathological changes that had occurred in the liver. Sections were then examined by light microscopy (Olympus, Japan).

2.10. Terminal deoxynucleotidyl transferase dUTP nick end labeling (TUNEL) assays

Portions of liver samples were embedded in paraffin and sliced into sections. The sections were incubated in 0.1% Triton X-100 for 8 min and then washed twice in PBS for 5 min. *In situ* labeling of apoptosis-induced DNA strand breaks (TUNEL assay) was performed using the *In Situ* Cell Death Detection Kit (Roche, Switzerland).

2.11. Western blot analysis

Total protein extracted from liver tissue was quantified using the BCA Protein Assay Kit (Applygen Technologies Inc. Beijing, China). Proteins were resolved by 10% sodium dodecyl sulfate-polyacrylamide gel electrophoresis and then transferred to polyvinylidene fluoride membranes. The membranes were incubated sequentially with appropriate primary antibodies and secondary antibodies. Immune complexes were visualized by super ECL detection reagent (Applygen, Beijing, China) and band intensities were determined using the Gel-Pro Analyzer 4.0 software (Media Cybernetics, USA). Primary antibodies against the following proteins were used: β-actin, GAPDH, BCL-2, BAX, and cytochrome *c* (Santa Cruz Biotechnology Inc., USA), and Caspase 3 (Cell Signaling Technology, USA).

2.12. Statistical analysis

All data were expressed as the mean $\pm$ standard deviation (SD). Differences between groups were assessed using Student's *t*-test. *P* values less than 0.05 were considered statistically significant.

3. Results

3.1. Induction of chronic immune liver fibrosis in a rat model via porcine serum administration

At 6 weeks post-PS injection, the HA and PIIINP levels in the treated group were significantly increased as compared to those in the control group, and continued to increase thereafter. The hepatic Hyp levels also increased between 6 and 11 weeks post-porcine serum injection (Fig. 1a). Ultrasound imaging is a popular and noninvasive tool that is frequently used to diagnose liver diseases. As shown in Fig. 1b, liver surfaces in the control group showed smooth, thin and regular hyperechogenic features. At 6 weeks post-PS injection, however, the liver surfaces showed irregularities and increased echo intensities. At 8–11 weeks post-treatment, the liver surfaces demonstrated irregular, spotty surfaces and severely coarse echoes, indicating that the rats injected with porcine serum had developed fibrosis. The histopathological changes in the liver induced by porcine serum are shown in Fig. 1c. The structures of the control-group livers were clear, with consistent hepatocyte sizes and no denaturation or necrosis observed. At 6 weeks post-porcine serum treatment, the livers showed portal inflammation and ballooning degeneration of hepatocytes, representing an early stage of hepatic fibrosis. At 8 weeks post-porcine serum injection, the liver tissues showed fibrous tissue hyperplasia, bile duct proliferation, and inflammatory cell infiltration. At 10 weeks post-porcine serum injection, the liver tissues revealed pseudolobule formations and fibrotic septum formation.

3.2. Acute liver failure induced by D-gal/LPS treatment via liver cirrhosis

The fibrotic/cirrhotic rats generated by porcine serum were injected D-gal and LPS to induce ACLF. The survival times of ACLF rats are shown in Fig. 2a. Only one rat died within 7.5 h, most rats died within 13 h, and the mortality was 80% within 48 h. No rats with cirrhosis died throughout the experiment.

ALT and AST are classical biomarkers of liver injury. Compared to the group before D-gal/LPS induction (0 h, cirrhosis rats), the serum levels of ALT and AST markedly increased at 4 h after induction by D-gal/LPS, whereas the levels significantly decreased at 8 h and 12 h post-treatment. The levels of TBiL, DBiL and TBA increased substantially at 4 h and peaked at 12 h post-treatment (Fig. 2b).

Prothrombin time (PT), *i.e.*, the time for the plasma clotting, is also used to determine liver function, as liver functional abnormalities result in deficiencies of coagulation factors. There were no rats whose PT exceeded 80 s in the normal rat and cirrhotic groups, with the mean PT being 17 and 21 s respectively. The clotting time markedly increased at 4 h and at 8–12 h post-induction by D-gal/LPS (Fig. 2c). At 8–12 h post-induction, the clotting times of ACLF rats were all longer than 80 s.

The levels of the pro-inflammatory cytokines TNF-α and IL-6 are shown in Fig. 2d. Our results demonstrated that normal rats and cirrhotic rats showed very low TNF-α and IL-6 production. After induction by D-gal/LPS, the serum levels TNF-α and IL-6 increased significantly compared to normal rats and cirrhotic rats.

As shown in Fig. 2e, no significant differences were observed in plasma ammonia levels between the control and cirrhotic groups. After D-gal/LPS injection, the level of plasma ammonia significantly increased at 8 h and 12 h post-treatment compared to those measured in the control and cirrhotic groups.

The histological features in the livers of control animals revealed a normal liver lobular architecture and cell structure (Fig. 2f). At 4 h post-treatment of D-gal/LPS, ballooning degeneration of hepatocytes was found, and some areas of necrosis were observed. At 12 h post- treatment of D-gal/LPS, liver cells showed obvious necrosis.

3.3. *Severe hepatocyte apoptosis induced by combined D-gal/LPS treatment in ACLF rats*

Hepatic levels of apoptosis-related proteins were detected by Western blot analysis (Fig. 3a–d). The results showed marked increases in the expression of BAX, while that of BCL-2 decreased markedly. The expression of cytochrome *c* peaked at 8 h, but deceased at 12 h post-treatment. The expression of cleaved caspase-3 peaked 4 h post-treatment of D-gal/LPS and decreased subsequently.

TUNEL assay results are shown in Fig. 3e. Apoptosis was low in the control group. Compared to the control group, a small number of hepatocytes showed apoptosis in the ACLF group before D-gal/LPS induction (0 h). However, apoptosis increased markedly over time. Twelve hours after D-gal/LPS treatment, numerous TUNEL-positive cells were observed in the outer nuclear layer, suggesting dramatic cell death and tissue damage.

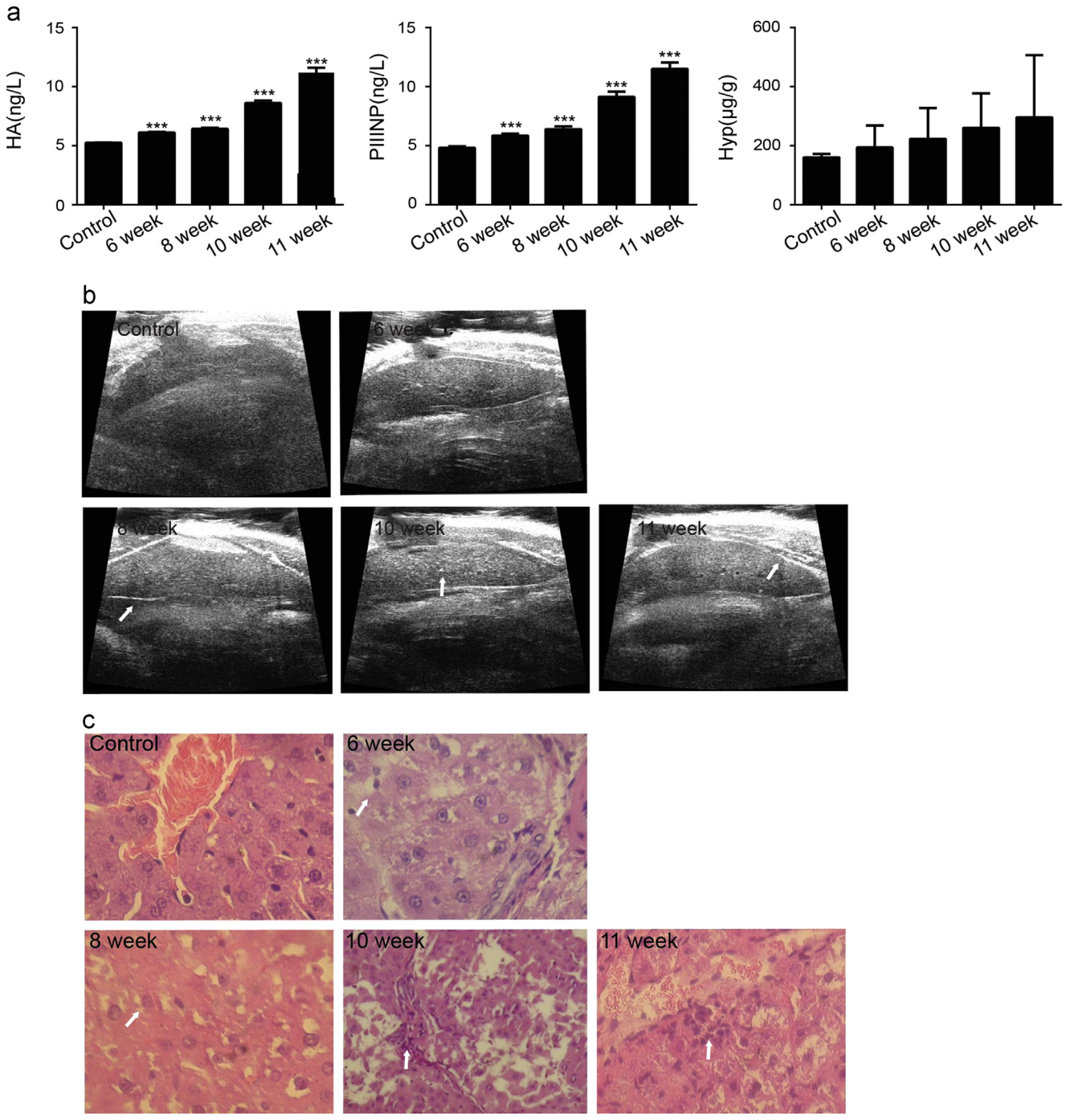

Figure 1 Rats were injected with porcine serum for 11 weeks. (a) Changes in hydroxyproline, hyaluronic acid and N-procollagen type III peptide concentrations ($n=5$). (b) Ultrasound image of the livers in rats injected with porcine serum (transverse section). (c) H&E staining to illustrate the formation of liver fibrosis induced by porcine serum in rats (200 ×). $^{***}P < 0.001$ compared with the control group.

4. Discussion

ACLF is a severe, life-threatening condition found in patients with previously diagnosed or undiagnosed chronic liver disease who have an acute deterioration of liver function and an increased risk of multi-organ failure and death over a short period, following a precipitating event such as liver injury or infection[2,10]. The mechanism whereby patients with cirrhosis experience rapid liver deterioration, with acutely worsening liver functions following a superimposed inflammatory insult remains

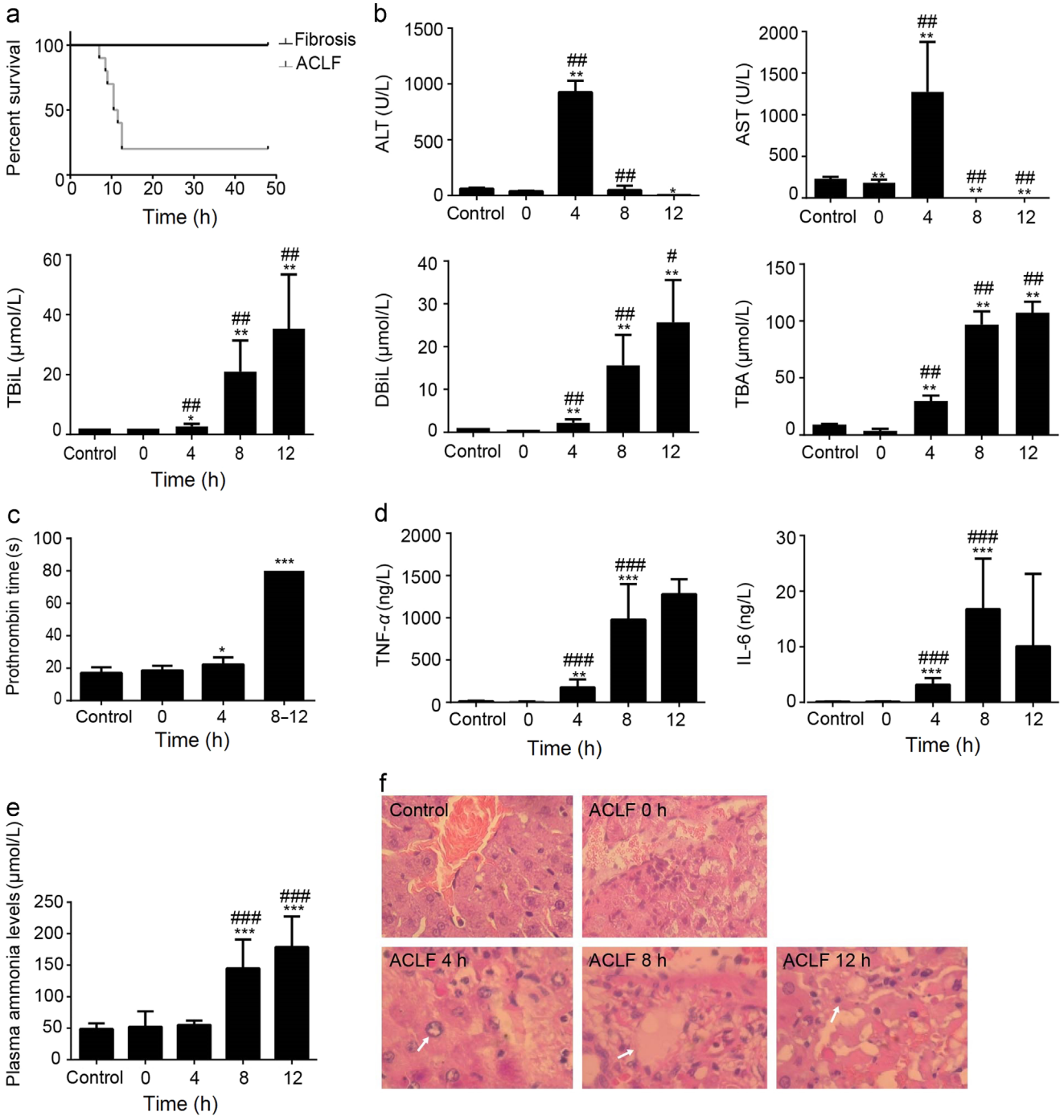

Figure 2 Rats were subjected to D-gal/LPS injection after porcine serum injection for 11 weeks. (a) Survival rates of ACLF rats ($n=10$). (b) Changes in serum biochemical indices after D-gal/LPS treatment in ACLF rats ($n=3$–5). (c) Prothrombin time in fibrotic rats following treatment with D-gal/LPS in ACLF rats (n = 3–5). (d) The plasma levels of TNF-α and IL-6 after D-gal/LPS treatment in ACLF rats ($n=5$). (e) The plasma levels of ammonia after D-gal/LPS treatment in ACLF rats ($n=5$). (f) H&E staining was performed to evaluate the effects of liver failure induced by D-gal/LPS in ACLF rats (200 ×). $^{*}P < 0.05$, $^{**}P < 0.01$, $^{***}P < 0.001$ compared with the control group. $P < 0.05$, $P < 0.01$, $P < 0.001$ compared with the ACLF animals before D-gal/LPS injection (0 h).

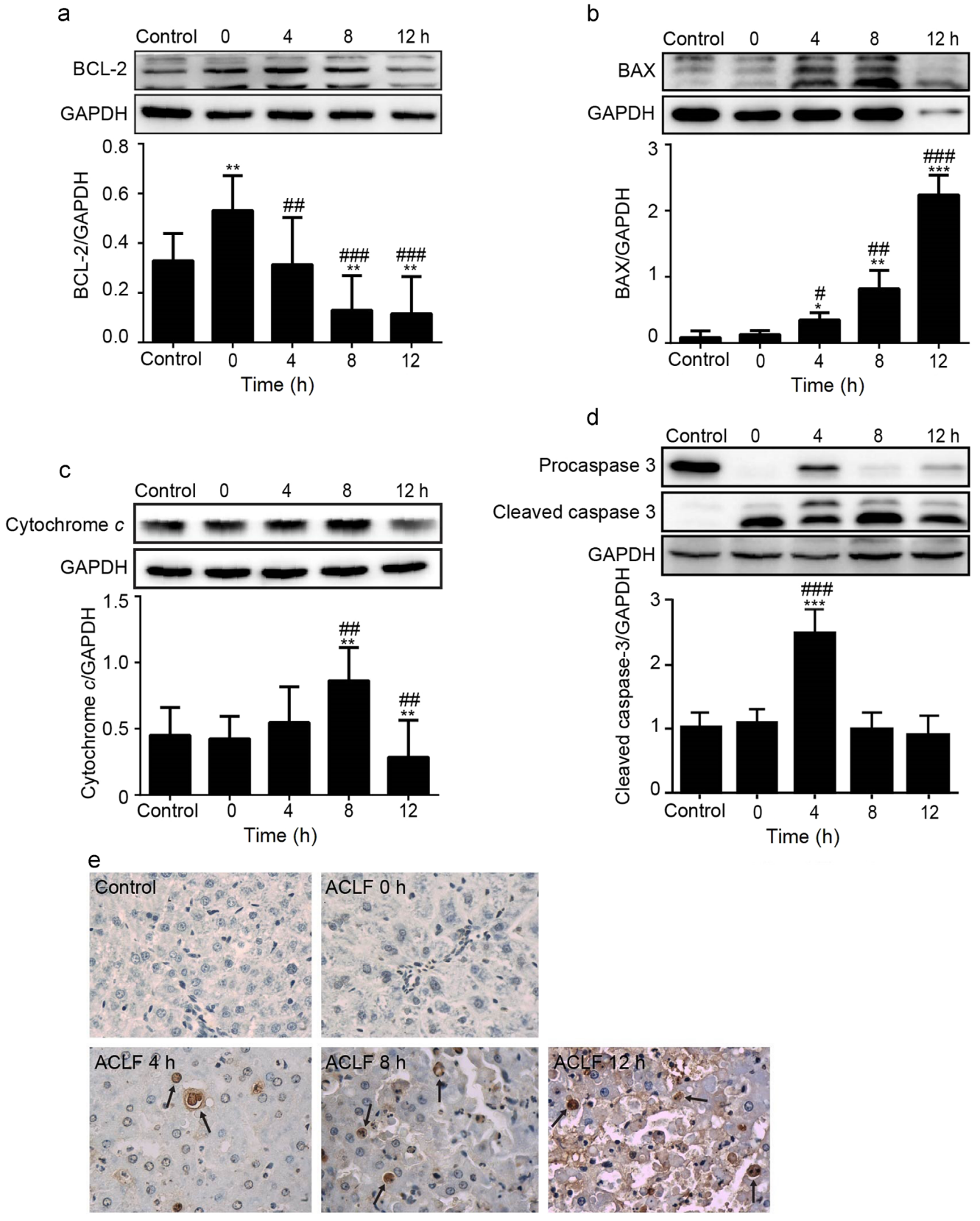

Figure 3 Expression of the mitochondrial apoptosis pathway–related protein in the ACLF rat model using Western blot analysis: (a) BCL-2; (b) BAX; (c) cytochrome *c*; (d) cleaved caspase-3; and (e) Terminal deoxynucleotidyl-transferase dUTP nick-end labeling (TUNEL) assays performed to evaluate apoptosis after D-gal/LPS treatment in ACLF rats (400 ×). $^{*}P < 0.05$, $^{**}P < 0.01$, $^{***}P < 0.001$ compared with the control group; $P < 0.05$, $P < 0.01$, $P < 0.001$ compared with the ACLF animals before D-gal/LPS injection (0 h).

unclear. Furthermore, very limited data are currently available from applicable animal models simulating this pathophysiological process. Therefore, developing an ACLF model that can mimic these processes would aid in understanding the underlying mechanism of hepatic damage during ACLF development, which is necessary for generating novel drugs to treat such a devastating disease.

In this study, we developed a new ACLF model that mimics human ACLF as observed in clinical and laboratory settings, and which represents an improvement over existing animal models. According to the "two hit" theory[11], ACLF is induced by D-gal/LPS injection following liver fibrosis/cirrhosis induced by PS administration. Liver fibrosis induced by PS injection has been widely used in studying liver fibrosis[12,13]. Compared to the HSA-induced liver fibrosis model, our model offers an advantage in terms of simple operation. In addition, during the fibrosis-induction period, no animal died, while the HSA-induced model shows a relatively high mortality of 23%[14]. Our laboratory previously used HSA to establish a liver fibrosis model and the death rate was 30% (data not shown), which is consistent with literature reports. BDL and CCl_4 models are not consistent with the pathogenesis of ACLF. Moreover, the surgery required for BDL is complex, and the model is not stable, while our method serves as a stable, repeatable model and is similar to pathogenesis of ACLF in clinical settings. In the acute deterioration phase, D-gal/LPS was administered to exacerbate the pathophysiological processes of ACLF. LPS, a critical component of the cell membrane of Gram-negative bacteria, could activate kupffer cells *via* toll-like receptor 4 (TLR4)-mediated mitogen-activated protein kinases (MAPK) and nuclear factor-kappa B (NF-κB) signal pathways, and stimulate the production and release of inflammatory factors including TNF-α which will induce apoptosis and necrosis of hepatocytes[15]. D-Gal is an amino sugar that is selectively metabolized by hepatocytes, and which induces liver damage by depletion of the uridine triphosphate pool and thereby inhibits protein synthesis. With combined exposure to D-gal and LPS, D-gal specifically sensitizes the liver towards the cytotoxic effects of LPS, promoting the development of acute liver injury and possible death[16]. Hence, combined administration of D-gal/LPS has been widely used as to mimic the sequence of events in human hepatitis.

In our current animal model, we demonstrate that liver fibrosis/early-stage cirrhosis is induced following PS challenge, which is supported by the finding that the levels of HA and PIIINP increased substantially, and by the ultrasonic-testing and liver-histology results. Subsequent D-gal/LPS treatment caused acute focal necrosis, intermittent necrosis within 4 h, and sub-massive hepatic necrosis within 12 h. These observations were supported by the findings that levels of ALT and AST increased significantly and decreased afterwards, and that TBiL, DBiL, and TBA levels increased markedly. Furthermore, a high rate of mortality was observed within a short period following D-gal/LPS treatment, starting after 7.5 h and reaching 80% at 48 h, suggesting that our current model accurately reflects the clinical manifestations of ACLF.

Serum biochemical constituents, such as ALT, AST, TBiL, DBiL and TBA, are widely used to monitor liver functions in medical practice. ALT and AST are released into the bloodstream when the liver is damaged or diseased. Bilirubin is a breakdown product of hemoglobin. TBiL and DBiL are usually measured to screen for or monitor jaundice caused by liver or gall bladder dysfunction[17]. TBA is an exclusive index of liver function. The specificity, sensitivity, and stability of TBA measurements render it (for many hepatobiliary disorders) superior to conventional liver-function examinations[18]. In our current study, a significant change in the activities of serum enzymes and constituents was observed. At 4 h post-administration of D-gal/LPS, the levels of ALT, AST, TBiL, DBiL and TBA increased markedly, whereas at 8 h, the levels of ALT and AST decreased, and the level of TBiL, DBiL and TBA continuously increased. These data indicate the induction of sub-massive hepatic necrosis, which is consistent with the pathogenic processes of ACLF that are observed clinically.

In the clinic, ACLF patients are also found to have coagulation disorders. The liver plays an important role in hemostasis because many of the proteins involved in coagulation, antithrombosis, and fibrinolytic systems are synthesized in the liver. Thus, it is easy to understand how advanced liver diseases can disrupt hemostatic functions[19,20]. In this study, prothrombin time in ACLF markedly increased after acute D-gal/LPS treatment. We also found increased plasma ammonia levels in ACLF rats. These two results are consistent with clinical research[21].

The main pathological feature of ACLF is necrosis of numerous liver cells accompanied with inflammatory cell infiltration as the basis for chronic liver failure. We also observed a significant increase in the serum levels of TNF-α and IL-6 in ACLF rats, which are the important inflammatory cytokines of liver failure[9]. Given that liver cell apoptosis and necrosis may relate to increased TNF-α and IL-6 production, this further indicates that their livers were in an inflammatory condition.

TUNEL assay and histological analyses of liver samples were performed to further evaluate the features of the new ACLF model. Histopathological findings showed that ballooning degeneration of hepatocytes and false liver acini developed at 4 h and the degree of inflammation and necrosis was aggravated at 8 h following the D-gal/LPS attack. From the pathophysiological point of view, our current model may closely mimic the symptoms found in ACLF patients with hepatitis B infection. The TUNEL assay results also revealed that numerous hepatocytes underwent apoptosis over time, which is consistent with the histopathology results.

Apoptosis is a cell-suicide mechanism that enables multicellular organisms to maintain homeostasis and eliminate individual cells that threaten the organism's survival. Depending on the type of stimulus, apoptosis can be propagated by an extrinsic pathway or intrinsic pathway. It is well known that BCL-2 is an apoptosis inhibitor and that proteins of the BCL-2 family constitute an important control mechanism in regulating apoptosis[22]. BAX is a pro-apoptotic protein that functions by competing with BCL-2 in cells. A change in the BAX/BCL-2 ratio alters the susceptibility of cells to apoptosis[23]. Caspases are intracellular cysteine proteases that are important components in classical apoptosis. Caspase activation occurs in response to various types of mitochondrial damage and pro-apoptotic stimuli which cause cytochrome *c* release into the cytosol. Cytochrome *c* in turn activates caspase proteins[24]. We observed a marked increase in BAX expression, whereas expression of BCL-2 decreased markedly. Cleaved caspase-3 and cytochrome *c* were also overexpressed after D-gal/LPS administration for 4 h and 8 h. Our results suggest that the intrinsic apoptosis pathway is involved in the development of ACLF. The role of the extrinsic pathway remains to be elucidated. During this study, we observed that expression of proteins decreased after 12 h following the D-gal/LPS attack, which may be related to protein synthesis dysfunction in hepatocytes. In summary, we established a new rat model of ACLF which is useful and stable. Such a model enables investigation of the

pathophysiology of ACLF and evaluation of the efficacy of novel drugs. Although our model has advantages compared to the current models, it does not mimic fully the pathogenesis of ACLF, and further exploration is needed.

Acknowledgments

This work was supported by 863 program (No. 2014AA021101) from National High-tech R&D Program of China and the grants from National Sciences Foundation of China (Grant No. 81573487).

References

1. Sarin SK, Kumar A, Almeida JA, Chawla YK, Fan ST, Garg H, et al. Acute-on-chronic liver failure: consensus recommendations of the Asian Pacific Association for the study of the liver (APASL). *Hepatol Int* 2009;**3**:269–82.
2. Jalan R, Gines P, Olson JC, Mookerjee RP, Moreau R, Garcia-Tsao G, et al. Acute-on chronic liver failure. *J Hepatol* 2012;**57**:1336–48.
3. Jia JD, Zhuang H. A winning war against hepatitis B virus infection in China. *Chin Med J* 2007;**120**:2157–8.
4. Sen S, Williams R, Jalan R. The pathophysiological basis of acute-on-chronic liver failure. *Liver* 2002;**22**(Suppl. 2)S5–13.
5. Li X, Wang LK, Wang LW, Han XQ, Yang F, Gong ZJ. Blockade of high-mobility group box-1 ameliorates acute on chronic liver failure in rats. *Inflamm Res* 2013;**62**:703–9.
6. Kuhla A, Eipel C, Abshagen K, Siebert N, Menger MD, Vollmar B. Role of the perforin/granzyme cell death pathway in D-Gal/LPS-induced inflammatory liver injury. *Am J Physiol Gastrointest Liver Physiol* 2009;**296**:G1069–76.
7. Balasubramaniyan V, Dhar DK, Warner AE, Vivien Li WY, Amiri AF, Bright B, et al. Importance of Connexin-43 based gap junction in cirrhosis and acute-on-chronic liver failure. *J Hepatol* **58**:1194–200.
8. Hou W, Piao ZF, Zhang HY, Liu Z, Meng QH. The approaches for making acute-on-chronic liver failure in rat. *Chin J Exp Clin Virol* 2009;**23**:394–6.
9. Yang F, Li X, Wang LK, Wang LW, Han XQ, Zhang H, et al. Inhibitions of NF-κB and TNF-α result in differential effects in rats with acute on chronic liver failure induced by D-Gal and LPS. *Inflammation* 2014;**37**:848–57.
10. Moreau R, Jalan R, Gines P, Pavesi M, Angeli P, Cordoba J, et al. Acute-on-chronic liver failure is a distinct syndrome that develops in patients with acute decompensation of cirrhosis. *Gastroenterology* 2013;**144**:1426–37.
11. Amacher DE. Strategies for the early detection of drug-induced hepatic steatosis in preclinical drug safety evaluation studies. *Toxicology* 2011;**79**:10–8.
12. Zhong L, Wang X, Wang S, Yang L, Gao H, Yang C. The anti-fibrotic effect of bone morphogenic protein-7 (BMP-7) on liver fibrosis. *Int J Med Sci* 2013;**10**:441–50.
13. Huang YH, Chen YX, Zhang LJ, Chen ZX, Wang XZ. Hydrodynamics-based transfection of rat interleukin-10 gene attenuates porcine serum-induced liver fibrosis in rats by inhibiting the activation of hepatic stellate cells. *Int J Mol Med* 2014;**34**:677–86.
14. Dong Z, Liu J, Shen H, Ma H, Jia JD. Immune complex induced rat liver fibrosis model by intraperitoneal injection of human serum albumin. *Chin J Exp Clin Virol* 2006;**20**:12–5.
15. Wang LK, Wang LW, Li X, Han XQ, Gong ZJ. Ethyl pyruvate prevents inflammatory factors release and decreases intestinal permeability in rats with D-galactosamine–induced acute liver failure. *Hepatobiliary Pancreat Dis Int* 2013;**12**:180–8.
16. Liu H, Zhang W, Dong S, Song L, Zhao S, Wu C, et al. Protective effects of sea buckthorn polysaccharide extracts against LPS/D-GalN–induced acute liver failure in mice *via* suppressing TLR4-NF-κB signaling. *J Ethnopharmacol* 2015;**176**:69–78.
17. Ding Y, Zhao L, Mei H, Huang ZH, Zhang SL. Alterations of biliary biochemical constituents and cytokines in infantile hepatitis syndrome. *World J Gastroenterol* 2006;**12**:7038–41.
18. Tomer G, Ananthanarayanan M, Weymann A, Balasubramanian N, Suchy FJ. Differential developmental regulation of rat liver canalicular membrane transporters Bsep and Mrp2. *Pediatr Res* 2003;**53**:288–94.
19. Olaleye MT, Amobonye AE, Komolafe K, Akinmoladun AC. Protective effects of *Parinari curatellifolia* flavonoids against acetaminophen-induced hepatic necrosis in rats. *Saudi J Biol Sci* 2014;**21**:486–92.
20. Hoffman M. Coagulation in liver disease. *Semin Thromb Hemost* 2015;**41**:447–54.
21. Shu JC, Li QY, Yang QH, Zhang WR, Li ME, Zhang XY, et al. Ultrastructural changes of duodenal mucosa and their significance in patients with liver cirrhosis. *Chin J Hepatol* 2007;**15**:254–7.
22. Kirkin V, Joos S, Zörnig M. The role of Bcl-2 family members in tumorigenesis. *Biochim Biophys Acta* 2004;**1644**:229–49.
23. Jendrossek V. The intrinsic apoptosis pathways as a target in anticancer therapy. *Curr Pharm Biotechnol* 2012;**13**:1426–38.
24. Jiang L, Wang L, Chen L, Cai GH, Ren QY, Chen JZ, et al. As_2O_3 induces apoptosis in human hepatocellular carcinoma HepG2 cells through a ROS-mediated mitochondrial pathway and activation of caspases. *Int J Clin Exp Med* 2015;**8**:2190–6.